Surv Geophys (2010) 31:225–245
DOI 10.1007/s10712-009-9087-x

ORIGINAL PAPER

Numerical Modelling in Geo-Electromagnetics: Advances and Challenges

Ralph-Uwe Börner

Received: 15 January 2009 / Accepted: 5 October 2009 / Published online: 28 October 2009

Abstract During the last decade, tremendous advances have been observed in the broad field of numerical modelling for geo-electromagnetic applications. This trend received support due to increasing industrial needs, mainly caused by hydrocarbon and ore exploration industry. On the other hand, the increasing reliability and accuracy of data acquisition techniques further spurs this development. In this review, we will focus on advances and challenges in numerical modelling in geo-electromagnetics. We review recent developments in the discrete solution of the 3-D induction problem in the time and frequency domains. Particularly, advantages and disadvantages of the common numerical techniques for solving partial differential equations such as the Finite Difference and Finite Element methods will be considered.

Keywords Numerical modelling · Finite differences · Finite elements · Frequency-domain methods · Time-domain methods

1 Introduction

The achievements of three-dimensional modelling and inversion have recently been reviewed in a comprehensive paper by Avdeev (2005). In this review paper, we particularly consider the numerical solution of the three-dimensional geo-electromagnetic induction problem in the time- and frequency-domain. The most promising methods disposable for the discretization of Maxwell's equations in space and time will be discussed. Deliberately, this review shall be restricted to the Finite Difference (FD) and Finite Element (FE) spatial discretization methods, knowingly ignoring the vast field of Integral Equation methods, thin-sheet solutions, etc. Also, 3-D inversion strategies will only be considered as algorithms where forward modelling routines account for most of

Invited talk presented at the 19th Workshop on Electromagnetic Induction in the Earth, Beijing, China, 2008.

R.-U. Börner (✉)
Institute of Geophysics, Technische Universität Bergakademie Freiberg, Freiberg, Germany
e-mail: rub@geophysik.tu-freiberg.de

the total computing time. Hence, it shall be emphasized that recent developments in 3-D modelling techniques will have a tremendous impact on the development of inversion strategies. This paper is organized as follows: First, a brief introduction of the theory of the continuous physical problem of geo-electromagnetic induction will be given. Second, discretization methods in space and time will be discussed. The numerical methods available for the solution of the large equation systems arising from the spatial discretization of the partial differential equations will be presented in section 3. Most challenging problems of code efficiency and speed will be addressed in the last section.

2 Discretization in Space and Time

The behaviour of electromagnetic fields in the time domain can be described by an initial boundary value problem for Maxwell's equations in quasi-static approximation

$$\nabla \times \mathbf{h} - \sigma \mathbf{e} = \mathbf{j}^e, \tag{1a}$$

$$\partial_t \mathbf{b} + \nabla \times \mathbf{e} = \mathbf{0} \tag{1b}$$

$$\nabla \cdot \mathbf{b} = 0, \tag{1c}$$

$$\nabla \cdot \mathbf{d} = \rho, \tag{1d}$$

where we denote by $\mathbf{e}(\mathbf{r}, t)$ the electric field, $\mathbf{h}(\mathbf{r}, t)$ the magnetic field, $\mathbf{b}(\mathbf{r}, t) = \mu\,\mathbf{h}(\mathbf{r}, t)$ the magnetic flux density, $\mathbf{d}(\mathbf{r}, t)$ is the electric displacement, $\mu(\mathbf{r})$ is the magnetic permeability, $\rho(\mathbf{r})$ a volume charge density, and $\mathbf{j}^e(\mathbf{r}, t)$ external source current density, respectively. The spatial variable $\mathbf{r}$ is restricted to a computational domain $\Omega \subset \mathbb{R}^3$ bounded by an artificial boundary Γ, along which appropriate boundary conditions on the tangential components of the fields are imposed, whereas $t \in \mathbb{R}$. The forcing results from a known stationary transmitter source with a driving current which is shut off at time $t = 0$, and hence of the form

$$\mathbf{j}^e(\mathbf{r}, t) = \mathbf{q}(\mathbf{r})H(-t) \tag{2}$$

with the vector field $\mathbf{q}$ denoting the spatial current pattern and H being the Heaviside step function. The Earth's electrical conductivity is denoted by the parameter $\sigma(\mathbf{r})$. After eliminating $\mathbf{b}$ from (1a–1d) we obtain the second order partial differential equation

$$\nabla \times (\mu^{-1} \nabla \times \mathbf{e}) + \partial_t \sigma \mathbf{e} = -\partial_t \mathbf{j}^e \quad \text{in } \Omega \tag{3a}$$

for the electric field, which—for the sake of brevity—we complete with the perfect conductor boundary condition

$$\mathbf{n} \times \mathbf{e} = 0 \quad \text{on } \Gamma, \tag{3b}$$

at the outer walls of the model with $\mathbf{n}$ introduced as the outer normal vector on Γ. Obviously, there are cases which require more general expressions for the electric fields at the outer boundaries, which would then take the general form $\mathbf{n} \times \mathbf{e} = \mathbf{n} \times \mathbf{e}_0$ on Γ (Fig. 1).

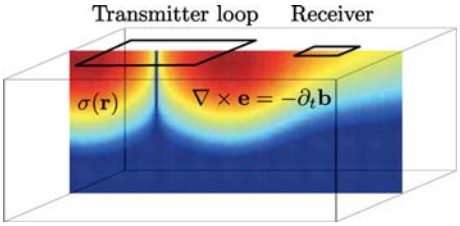

Fig. 1 Schematic representation of the continuous electric field a short time after the shut-off of a driving electric current in the transmitter loop. The voltage induced in the receiver coil is proportional to the time rate of change of the magnetic induction

Switching to the frequency domain, we introduce the Fourier transform pair

$$\mathbf{e}(t) = \frac{1}{2\pi} \int_{-\infty}^{\infty} \mathbf{E}(\omega) \mathrm{e}^{i\omega t} \mathrm{d}\omega, \tag{4a}$$

$$\mathbf{E}(\omega) = \int_{-\infty}^{\infty} \mathbf{e}(t) \mathrm{e}^{-i\omega t} \mathrm{d}t, \tag{4b}$$

with ω denoting angular frequency. The representation (4a) can be interpreted as a synthesis of the electric field $\mathbf{e}(t)$ from weighted time-harmonic electric partial waves $\mathbf{E}(\omega)$, whereas (4b) determines the frequency content of the time-dependent electric field $\mathbf{e}$. We thus obtain the Fourier transformed version

$$\nabla \times (\mu^{-1} \nabla \times \mathbf{E}) + i\omega\sigma\mathbf{E} = \mathbf{q} \quad \text{in } \Omega, \tag{5a}$$

$$\mathbf{n} \times \mathbf{E} = 0 \quad \text{on } \Gamma, \tag{5b}$$

of (3a) and (3b). Note that a simple boundary condition like (5b) may introduce errors in the numerical solution which may severely deviate from an asymptotic behaviour at the boundaries as it is required e.g. in the case of magnetotellurics (MT). In the MT case, the boundary values for the electric fields can be those arising from electromagnetic induction in a layered Earth. This approach is sufficiently accurate when the outer boundaries are several skin depths away from lateral inhomogeneities of electrical conductivity.

In the following, the recent developments of numerical techniques for the spatial and time discretization of either the first-order system (1a–1d), or the second-order partial differential equations (3a, 3b) or (5a, 5b) will be reviewed.

2.1 Spatial Discretization

2.1.1 Finite Difference Methods

Due to their comparably low implementational effort, FD techniques have been extensively used in solving three-dimensional time-domain, frequency-domain, and DC resistivity modelling problems. Wang and Hohmann (1993) have presented a 3-D FD algorithm based on a discretization of the first-order system of Maxwell's equations on a staggered grid, which has been introduced by Yee (1966). Staggered grids have since then been favored by many authors (e.g. Druskin and Knizhnerman 1988; Commer and Newman 2004; Mulder et al. 2008) for simulating the time evolution of diffusive EM fields. In the frequency

domain, the FD and related Finite Volume (FV) discretization techniques have been employed for the simulation of MT (see, e.g., Jones and Pascoe 1971; Smith and Booker 1991; Mackie et al. 1993), CSEM (see, e.g., Haber et al. 2000; Haber and Ascher 2001; Weiss and Constable 2006; Newman and Alumbaugh 1995), and DC resistivity (Dey and Morrison, 1979; Spitzer 1995) methods.

The application of FD methods to calculate the response of anisotropic structures have been reported by Weidelt (1999); Weiss and Newman (2002, 2003). Davydycheva et al. (2003) have introduced a material averaging scheme (Moskow et al. 1999), that does not only require the grid spacing to be small, but also minimizes the error at the receiver locations and improves the approximation of the boundary conditions at infinity by incorporating a spectrally optimal grid refinement strategy.

Haber and Heldmann (2007) developed an OcTree discretization of Maxwell's equations in the quasi-static regime, and a multigrid solver. The benefit of such strategies is twofold: First, an adaptive local grid refinement can be achieved; second, a generation of nested grid hierarchies can be utilized for multigrid methods.

For the construction of a FD discretization, consider a tensor-product Cartesian grid with nodes at positions (x_k, y_l, z_m) with $k = 0, \ldots, N_x$, $l = 0, \ldots, N_y$, $m = 0, \ldots, N_z$. There are $N_x \times N_y \times N_z$ cells with these nodes as vertices (Fig. 2). Within a Yee cell, the electric field components are assumed to be edge-averaged, whereas the face-averaged magnetic field components are obtained by taking the curl of the electric field on elementary loops (Figs. 3 and 4).

Discretization of (5a, 5b) yields a system of linear equations

$$(\mathbf{K} + i\omega\mathbf{M})\mathbf{u} = \mathbf{f} \tag{6}$$

where $\mathbf{K}$ and $\mathbf{M}$ represent the discrete forms of the curl-curl operator $\nabla \times \nabla \times (\cdot)$ and the conductivity term arising from $\sigma\,\mathbf{E}$ in (5a, 5b), respectively. The right-hand side $\mathbf{f}$ arises from the source current density $\mathbf{q}$ and/or enforced boundary conditions (5b). The solution vector $\mathbf{u}$ finally contains the unknowns, in our case the components of the electric field distributed over the edges of all staggered grid Yee cells. Note that the stiffness matrix $\mathbf{K}$ is real and sparse, whereas the mass matrix $i\omega\mathbf{M}$ is purely imaginary and diagonal. Figure 5 display the matrix $\mathbf{K}$ arising from discretizing (5a, 5b) on a tensor-product FD grid with perfectly conducting walls.

2.1.2 *Finite Element Methods*

The use of FE techniques in geo-electromagnetics dates back at least to Coggon (1971), who derived solutions to 2-D DC resistivity problems using linear triangular elements.

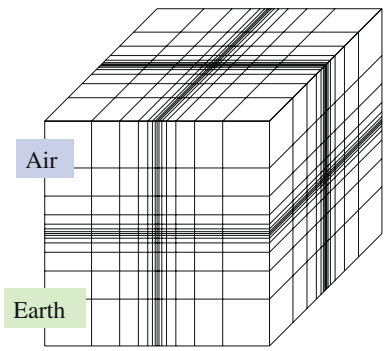

Fig. 2 A 3-D tensor-product grid with an irregular node spacing. The material properties are assumed to have constant values within each cell. To obtain a sufficiently accurate numerical solution, the grid spacing has to be very dense near a source, which in our case is located at the center of the cube

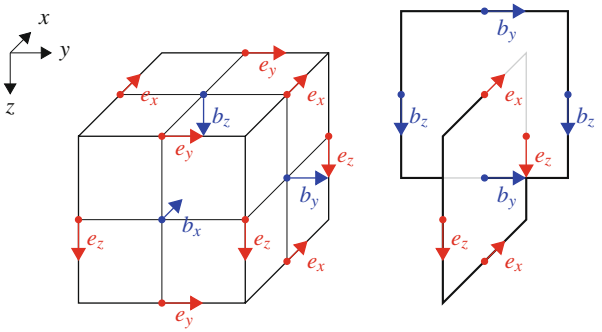

Fig. 3 Yee cell forming elementary loops, where electric and magnetic field components are assumed to be edge-averaged and face-averaged, respectively

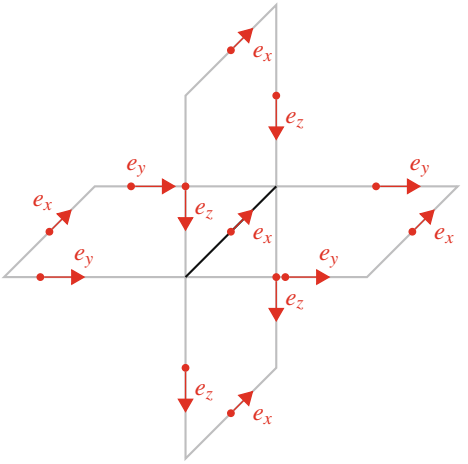

Fig. 4 The components of the electric field associated with one row of the discrete curl-curl operator

Since then, a number of authors have successfully used the FE method for electromagnetic modelling (Reddy et al. 1977; Pridmore et al. 1981; Livelybrooks 1993; Zunoubi et al. 1999; Zyserman and Santos 2000; Badea et al. 2001; Pain et al. 2002; Ruecker et al. 2006). One of the difficulties in the numerical modelling of electromagnetic field problems using FE is a possible jump of normal components across discontinuities of material properties.

Standard Lagrange elements, sometimes called *nodal* elements, which force all field components to be continuous across element boundaries, cannot reproduce the physical phenomenon of field discontinuities. We use the term *Lagrange element* for an approximation that is determined by values of the function being approximated at a finite number of points, in contrast to *Hermite elements*, which also depend on the interpolated function's derivatives.

This difficulty was resolved by the curl-conforming elements of Nédélec (Nédélec 1980, 1986), which are referred to as *edge elements* in the engineering literature since the lowest order elements of this family carry their degrees of freedom (dofs) at element edges. The FE subspaces of the Nédélec family perfectly capture the discontinuities of the electric and magnetic fields along material discontinuities.

The first to apply the edge elements to geoelectric problems were probably Jin et al. (1999), who developed a frequency-domain and time-domain FE solution using a Spectral Lanczos Decomposition Method (SLDM) for a small bandwidth of frequencies and very

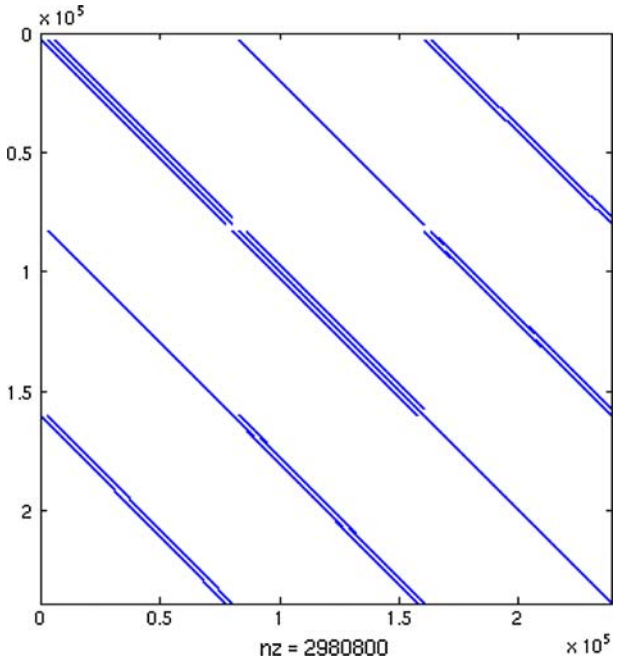

Fig. 5 Sparsity pattern of **K** arising from a FD grid consisting of $N_x = N_y = 54$ and $N_z = 28$ cells. The total number of unknowns excluding the outer domain boundaries is 239004, i.e. roughly $3 \cdot N_x N_y N_z$. Only 2980800 (roughly 0.005%) of the 239004 × 239004 matrix elements are in fact non-zero (nz)

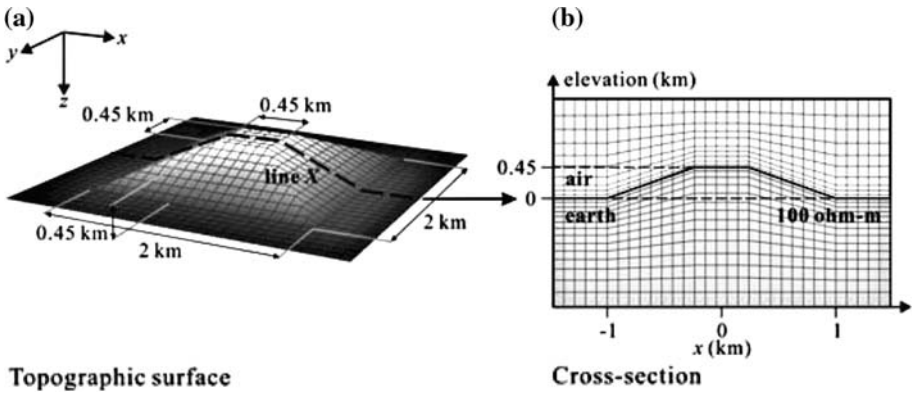

Fig. 6 3-D topographic model of a trapezoidal hill (Nam et al. 2007). Figure courtesy of Wiley-Blackwell

short times, respectively. Mitsuhata and Uchida (2004) have presented a FE approximation for computing MT responses for 3-D conductivity structures using a Helmholtz decomposition of the magnetic field into electric vector and magnetic scalar potentials with an appropriate gauge condition. Nam et al. (2007) have applied an edge FE method on hexahedral elements to calculate MT responses to 3-D topography (Fig. 6).

Using triangular or tetrahedral elements to mesh a computational domain allows for greater flexibility in the parametrization of conductivity structures avoiding staircasing at curved boundaries, such as arise with a terrain or sea-floor topography.

Key and Weiss (2006), Franke et al. (2007) have demonstrated the ability of adaptive Lagrange finite elements to approximate the MT response of complex geological 2-D structures. The implementation of adaptive mesh refinement strategies can yet further add to the flexibility of FE methods, since it allows for dramatic savings in the total number of degrees of freedom hence improving computational efficiency (Fig. 7).

Kong et al. (2008) have developed a 2.5-D FE method for marine controlled-source electromagnetic applications in stratified anisotropic media. They have adopted a scattered-field approach and, in doing so, were able to reduce the size of the computational domain and the total number of unknowns to be solved.

For the simulation of the magnetic field arising from induction in a spherical heterogeneous earth excited by ionospheric and magnetospheric current systems with complex spatiotemporal characteristics, such as magnetic storms, the method of spectral-finite elements provides a powerful tool. For this approach, two different types of parameterizations have been used simultaneously: A spherical harmonic parametrization of field variables, and the parametrization of the radial dependence of field quantities by piecewise linear functions (finite elements), hence the name spectral-finite elements (Martinec et al. 2003; Velimsky and Martinec 2005).

The issue of open, absorbing, or non-reflecting boundary conditions that have to be implemented on a truncating boundary, is one of the most intensively researched topics in the area of the numerical wave propagation. The most popular techniques include variations of Bérenger's Perfectly Matched Layers (PML) technique (Bérenger 1994), the Dirichlet-to-Neumann (DtN) method (Givoli 1992, 1999), and the method of Infinite Elements (Demkowicz and Pal 1998). Contrary to the idea of the PML, which modify Maxwell's equations within the boundary layers, the Infinite Elements discretizations work with the original equations and implement a decay function to approximate infinity for a bounded problem that extends to infinity.

For the construction of a 3-D vector FE approximation, we first express the boundary value problem (5) in variational or weak form (Monk 2003). The weak form requires the equality of both sides of (5a) in the inner product sense only. The $L^2(\Omega)$ inner product of two complex-valued vector fields **u** and **v** is defined as

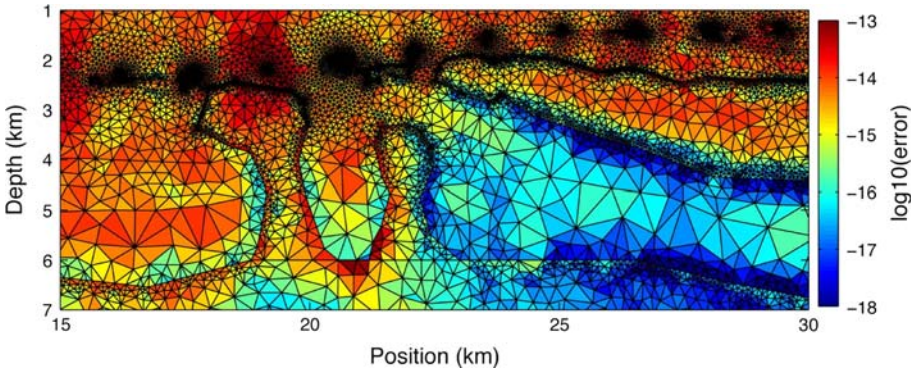

Fig. 7 Effect of an adaptive mesh refinement for the central part of a complex seafloor model. Shown is an error which is descriptive for the mesh quality (Key and Weiss 2006). Figure courtesy of Society of Exploration Geophysicists

$$(\mathbf{u},\mathbf{v}) = \int_{\Omega} \mathbf{u}\cdot\bar{\mathbf{v}}\,\mathrm{d}V \tag{7}$$

with $\bar{\mathbf{v}}$ denoting the complex conjugate of $\mathbf{v}$. Taking the inner product of (5a) with a sufficiently smooth vector field $\boldsymbol{\varphi}$ —called the test function—and integrating over Ω, we obtain after an integration by parts

$$\begin{aligned}&\int_{\Omega}\left[(\mu^{-1}\nabla\times\mathbf{E})\cdot(\nabla\times\bar{\boldsymbol{\varphi}}) + i\omega\sigma\mathbf{E}\cdot\bar{\boldsymbol{\varphi}}\right]\mathrm{d}V\\ &-\int_{\Gamma}(\mathbf{n}\times\bar{\boldsymbol{\varphi}})\cdot(\mu^{-1}\nabla\times\mathbf{E})\,\mathrm{d}A\\ &=\int_{\Omega}\mathbf{q}\cdot\bar{\boldsymbol{\varphi}}\,\mathrm{d}V.\end{aligned} \tag{8}$$

On Γ, the perfect conductor boundary condition (5b) gives no information about $(\mu^{-1}\nabla\times\mathbf{E})$, so we eliminate this integral by choosing $\boldsymbol{\varphi}$ such that $\mathbf{n}\times\boldsymbol{\varphi}=0$ on Γ. This is the standard way of enforcing the essential boundary condition (5b) in a variational setting.

Introducing the solution space $\mathcal{E} := \{\mathbf{v}\in\mathbf{H}(\mathrm{curl};\Omega) : \mathbf{n}\times\mathbf{v}=\mathbf{0} \text{ on } \Gamma\}$ in terms of the Sobolev space $\mathbf{H}(\mathrm{curl};\Omega) = \{\mathbf{v}\in L^2(\Omega)^3 : \nabla\times\mathbf{v}\in L^2(\Omega)^3\}$, the weak form of the boundary value problem finally reads:

Find $\mathbf{E}\in\mathcal{E}$ such that

$$\begin{aligned}&\int_{\Omega}\left[(\mu^{-1}\nabla\times\mathbf{E})\cdot\nabla\times\bar{\mathbf{v}} + i\omega\sigma\mathbf{E}\cdot\bar{\mathbf{v}}\right]\mathrm{d}V\\ &=\int_{\Omega}\mathbf{q}\cdot\bar{\mathbf{v}}\,\mathrm{d}V\end{aligned} \tag{9}$$

for all $\mathbf{v}\in\mathcal{E}$. Due to the homogeneous boundary condition (5b) the test functions can be chosen from the same space $\mathcal{E}$ (Fig. 8).

To construct a FE solution of the boundary value problem (5a, 5b) the domain Ω is partitioned into N_e simple geometrical subdomains, e.g. triangles for two-dimensional or tetrahedra (cf. Fig. 8) for three-dimensional problems, such that

$$\Omega = \bigcup_{e=1}^{N_e}\Omega_e. \tag{10}$$

The infinite-dimensional function space $\mathcal{E}$ introduced above is approximated by a finite N-dimensional function space $\mathcal{E}^h\subset\mathcal{E}$ of elementwise polynomial basis functions satisfying the homogeneous boundary condition (5b). The approximate electric field $\mathbf{E}^h\approx\mathbf{E}$ is defined as the solution of the discrete variational problem obtained by replacing $\mathcal{E}$ by $\mathcal{E}^h$ in (9) [cf. Monk (2003)].

To obtain the matrix form of (9), we express $\mathbf{E}^h$ as a linear combination of basis functions $\{\boldsymbol{\varphi}_i\}_{i=1}^{N}$ of $\mathcal{E}^h$, i.e.

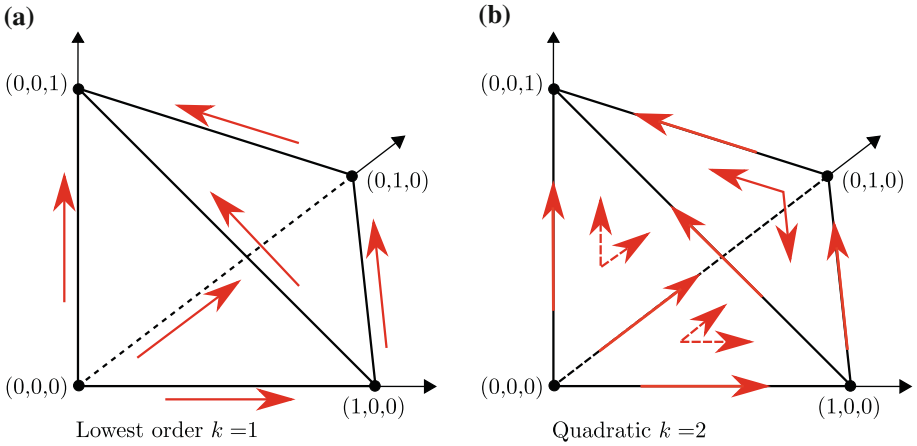

Fig. 8 Position of degrees of freedom (dofs) for lowest order linear **(a)** and quadratic **(b)** Nédélec elements. Note that in the linear case, the degrees of freedom are located at the edges of the tetrahedron, whereas in the quadratic case, there are two dofs associated with each edge, and two dofs associated with each face of the tetrahedron. Hence, the total number of dofs per tetrahedron is 6 in the linear case, and 20 in the quadratic case

$$\mathbf{E}(\mathbf{r}) = \sum_{i=1}^{N} E_i \boldsymbol{\varphi}_i(\mathbf{r}). \tag{11}$$

Testing against all functions in $\mathcal{E}^h$ is equivalent to testing against all basis functions $\boldsymbol{\varphi}_j, j = 1, \ldots, N$. Taking the j-th basis function as the test function and inserting (11) into (9) yields the jth row of a linear system of equations

$$(\mathbf{K} + i\omega\mathbf{M})\mathbf{u} = \mathbf{f} \tag{12}$$

for the unknown coefficients $E_i = [\mathbf{u}]_i$, $i = 1, \ldots, N$, where

$$[\mathbf{K}]_{j,i} = \int_{\Omega} (\mu^{-1} \nabla \times \boldsymbol{\varphi}_i) \cdot \nabla \times \bar{\boldsymbol{\varphi}}_j \mathrm{d}V, \tag{13}$$

$$[\mathbf{M}]_{j,i} = \int_{\Omega} \sigma \boldsymbol{\varphi}_i \cdot \bar{\boldsymbol{\varphi}}_j \mathrm{d}V, \tag{14}$$

$$[\mathbf{f}]_j = \int_{\Omega} \mathbf{q} \cdot \bar{\boldsymbol{\varphi}}_j \mathrm{d}V. \tag{15}$$

The matrices $\mathbf{K}$ and $\mathbf{M}$, known as *stiffness* and *mass matrices*, respectively, are large and sparse and, since μ and σ are real-valued quantities, consist of real entries. Figure 9 illustrates the sparseness properties of a stiffness matrix arising from a 3-D FE discretization scheme. Compared to a FD discretization, the relative increase of the number of non-zero elements in the stiffness matrix for the FE case arises from the fact, that each degree of freedom is spatially linked to more neighbors than in the FD case (Monk 1993).

For a given source vector $\mathbf{f}$ arising from the right-hand side of (5a), the solution vector $\mathbf{u} \in \mathbb{C}^N$ yields the approximation $\mathbf{E}^h$ of the electric field $\mathbf{E}$ we wish to determine. The

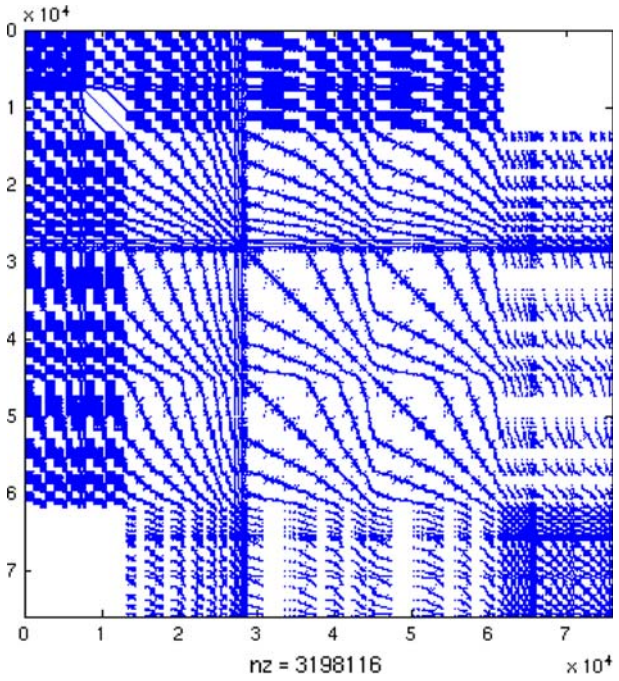

Fig. 9 Sparsity pattern of a typical stiffness matrix arising from a 3-D FE discretization using tetrahedral elements. A four-layer model including Air halfspace is considered. The underlying FE mesh consists of roughly 12300 tetrahedral elements, which for second-order edge elements corresponds to 75780 FE degrees of freedom. Only 3198116 (roughly 0.05%) of the 75780 × 75780 matrix elements are non-zero (nz)

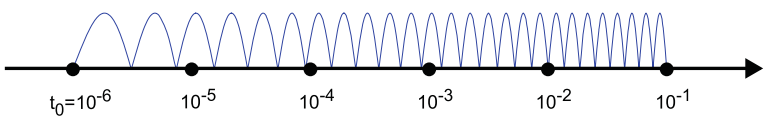

Fig. 10 On a logarithmically scaled time axis, the number of time steps required to run through a given time interval grows with later time stages

elements of the solution vector **u**, the degrees of freedom (dofs), are associated with the edges of the tetrahedra (cf. Fig. 8).

We note that the formulation presented here ensures the continuity of tangential electric field components along a common edge of adjacent tetrahedra by construction. Electric field components normal to common edges do not belong to the considered finite element function space, hence have to be projected onto that space, and therefore exhibit projection errors until the size of the finite elements becomes sufficiently small. There are powerful methods available which can be successfully used to reduce the errors generally once a finite element solution has been obtained. As the process of error reduction depends on previous results, it is called adaptive. Adaptive methods have been introduced in the late 1970s by Babuska and Rheinboldt (1978). Various procedures exist for the refinement of a finite element solutions. These fall into two categories: firstly, the *h*-refinement, in which the same class of elements continue to be used but are changed in

size, in some location made larger and in others smaller, to provide maximum economy in reaching the desired solution. Secondly, the *p*-refinement strategy continues to use the same element size and simply increases the order of polynomial used in their definition (Zienkiewicz et al. 2005).

2.2 Time Integration Techniques

Departing from (3a, 3b) and assuming a source current shut-off at time $t = 0$, the time evolution of the electric field at times $t > 0$ may be written as

$$\partial_t \mathbf{e} = -\sigma^{-1}\nabla \times \left(\mu^{-1}\nabla \times \mathbf{e}\right) \tag{16a}$$

$$\mathbf{e}(\mathbf{r}, t_0) = \mathbf{e}_0(\mathbf{r}), \quad t_0 > 0. \tag{16b}$$

The field $\mathbf{e}_0(\mathbf{r})$ represents the electric field known at a time t_0 after current shut-off.

We seek the electric field $\mathbf{e}(\mathbf{r}, t)$ due to induction caused by a shut-down of an magnetic field associated e.g. with a DC driven transmitter loop layed out at the Earth's surface.

There are several well suited techniques for integrating Maxwell's equations (1a–1d) or a diffusion equation (16a, 16b) in the time domain. The most prominent methods are

- Explicit DuFort-Frankel time-stepping schemes,
- Implicit schemes,
- Matrix exponentials and Lanczos reduction,
- Fourier transform based methods.

In the following, I will present the most important features of these approaches.

2.2.1 Explicit Schemes

The most basic explicit method for integrating ordinary or partial differential equations with initial values is the Euler method. The time derivative in (16a, 16b) is replaced by its first oder approximation

$$\partial_t \mathbf{e} \approx \frac{\mathbf{e}^{(\mathrm{n}+1)} - \mathbf{e}^{(n)}}{t^{(\mathrm{n}+1)} - t^{(n)}}$$

yielding

$$\mathbf{e}^{(\mathrm{n}+1)} = \mathbf{e}^{(\mathrm{n})} - \sigma^{-1}\nabla \times \left(\mu^{-1}\nabla \times \mathbf{e}^{(\mathrm{n})}\right) \Delta t,$$

where Δt is the time step $t^{(\mathrm{n}+1)} - t^{(\mathrm{n})}$. It is well known that the Euler method is stable only if the time step Δt is sufficiently small (Fig. 10). If Δ denotes the grid spacing, then for a homogeneous full space, the condition $\Delta t \leq \mu\sigma\, \Delta^2 / 4$ has to be satisfied.

Wang and Hohmann (1993) have overcome difficulties which might be arising in solving the second-order equation (16a, 16b) by proposing to solve the coupled first-order system of Maxwell's equations

$$\gamma \partial_t \mathbf{e} = -\sigma \mathbf{e} + \mu^{-1}\nabla \times \mathbf{b} \tag{17a}$$

$$\partial_t \mathbf{b} = -\nabla \times \mathbf{e}. \tag{17b}$$

Oristaglio and Hohmann (1984), Wang and Hohmann (1993), Commer and Newman (2004) follow the method of DuFort and Frankel (1953) and introduce a non-physical

fictitious displacement current term $\gamma\partial_t\mathbf{e}$, which has previously been neglected in the quasi-static approximation (1a). If $\Delta_{\min}$ is the smallest grid spacing, the DuFort–Frankel stability criterion is met if

$$\gamma \geq \frac{3}{\mu}\left(\frac{\Delta t}{\Delta_{\min}}\right)^2.$$

The fields remain diffusive for time steps obeying

$$\Delta t \ll \sqrt{\mu\sigma_{\min} t/6}\,\Delta_{\min}. \tag{18}$$

Note that the size of the time steps can increase with time.

The relation (18) indicates that the size of the time step is proportional to the square root of the smallest electrical conductivity $\sigma_{\min}$ within the computational domain. To circumvent unnecessary small time steps, an integral boundary condition relating the Dirichlet boundary condition to a Neumann boundary condition at the Earth's surface can be applied. Such a Dirichlet-to-Neumann (DtN) mapping restricts the size of the computational domain, or, as is the case in TEM simulations, enables the truncation of the infinite outer domain to allow for computations in a finite domain. The DtN mapping is non-local in space.

These non-local boundary conditions are implemented using a Fast Fourier transform (FFT), where an infinite summation has to be approximated by a finite summation. Since grid spacings usually grow towards the outer boundaries of the computational domain, a FFT cannot be applied directly to the discrete field components at the Earth's surface. Instead, the field components given on a graded grid have to be interpolated onto a regular, equidistant grid with an appropriate spatial sampling interval. This procedure significantly increases the computational load required to perform a single time step, since the numerical complexity of the required 2-D FFT operation is $\mathcal{O}(n^2 \log_2 n)$ when n is the number of samples in one horizontal direction. As reported by Commer and Newman (2004), a parallelization of the FFT does not yield the desired savings due to the overhead resulting from passing of variables between the nodes of the parallel architecture. However, there exists an appealing variant of the FFT on non-equidistant grids (Potts et al. 2001), which has the potential to overcome the aforementioned limitations while not exceeding the numerical complexity of a FFT. The actual suitability of such non-equidistant FFT algorithms has yet to be proved for 3-D TEM simulations.

2.2.2 *Implicit Schemes*

Haber et al. (2007) have solved the TEM forward problem using a Finite Volume method in the spatial domain and a Backward Euler implicit method in the time domain. The backward differentiation formula (BDF) is a family of implicit methods for the numerical integration of ordinary differential equations. They are linear multi-step methods that, for a given function and time, approximate the derivative of that function using information from already computed times, thereby increasing the accuracy of the approximation. These methods are especially useful for the solution of stiff differential equations. An equation is stiff, if certain numerical methods require a significant reduction of the size of the time steps to obtain a sufficiently stable solution. Using a backward Euler in time, an update of the electric and magnetic fields can be achieved by

$$\nabla \times \mathbf{e}^{(n+1)} + \mu \frac{\mathbf{h}^{(n+1)} - \mathbf{h}^{(n)}}{\Delta t} = 0 \tag{19a}$$

$$\nabla \times \mathbf{h}^{(n+1)} - \sigma \mathbf{e}^{(n+1)} - \varepsilon \frac{\mathbf{e}^{(n+1)} - \mathbf{e}^{(n)}}{\Delta t} = \mathbf{s}^{(n+1)}. \tag{19b}$$

The superscripts denote the discrete time level, such that $t_n = n\,\Delta t$, and solution quantities at $n + 1$ being unknown while those at n being known. The known time-dependent source term $\mathbf{s}(\mathbf{r}, t)$ at time step $n + 1$ is indicated by $\mathbf{s}^{(n+1)}$. After eliminating $\mathbf{e}^{(n+1)}$ from the above equations, a formulation for the update of the magnetic field can be derived as follows:

$$\nabla \times (\sigma + \varepsilon \Delta t^{-1})^{-1} \nabla \times \mathbf{h}^{(n+1)} - \nabla \mu^{-1} (\sigma + \varepsilon \Delta t^{-1})^{-1} \nabla \cdot \mathbf{h}^{(n+1)} + \mu \Delta t^{-1} \mathbf{h}^{(n+1)} = \mathbf{rhs}^{(n+1)}. \tag{20}$$

The term **rhs** is a function of the source at time step $n + 1$ as well as the electric and magnetic fields at the previous time step n, hence

$$\mathbf{rhs}^{(n+1)} = \nabla \times \left((\sigma + \varepsilon \Delta t^{-1})^{-1} \mathbf{s}^{(n+1)} - \mathbf{e}^{(n)} \right) + \mu \Delta t^{-1} \mathbf{h}^{(n)}. \tag{21}$$

When the conductivity is very small and the time step is large, the above system can be nearly singular. An appropriate method to stabilize the system is to introduce an additional condition on the magnetic field, namely the divergence free condition $\nabla \cdot \mu\, \mathbf{h} = 0$. Therefore, the term $\nabla \mu^{-1} (\sigma + \varepsilon \Delta t^{-1})^{-1} \nabla \cdot \mathbf{h}^{(n+1)}$ in (20) does not change the solution while numerically stabilizing the system. After discretization in space, a linear system of the form

$$\mathbf{A}(\sigma) \mathbf{h}^{(n+1)} = (\mathbf{C}(\sigma, \Delta t) + \mathbf{M}(\mu, \Delta t)) \mathbf{h}^{(n+1)} = \mathbf{rhs}^{(n+1)} \tag{22}$$

has to be solved for $\mathbf{h}^{(n+1)}$. The matrices **C** and **M** are the discretized form of the action of the operators in equation (20) on $\mathbf{h}^{(n+1)}$. While removing the stability constraint on the time step, implicit methods require the solution of large linear system of equations at each time step.

A Cholesky factorization of the symmetric and positive definite matrix $\mathbf{A}(\sigma)$ appears to be attractive (Haber et al. 2006), when the time step remains the same in (20). Once such a factorization is available, multiple sources can be handled at almost no additional cost. Thus, the approach reported is useful even for multiple sources which is most important for a practical inversion of TEM data (Haber et al. 2007).

2.2.3 Matrix Exponentials

A suitable discretization of (16a, 16b) yields the linear inital value problem

$$\partial_t \mathbf{e} = \mathbf{A}\mathbf{e}, \quad \mathbf{e}(t_0) = \mathbf{e}_0 \tag{23}$$

for $\mathbf{e}(t)$, $t > t_0$. The vector $\mathbf{e}_0$ is the discretized electric field at time $t = t_0 > 0$ after current shut-off. The matrix **A** is the discrete action of the curl-curl operator on the right-hand side of (16a). It has similar properties to the stiffness matrix **K** in (6), such as it is large, sparse, and symmetric or symmetrizable. Therefore, matrix-vector products with **A** can be carried out inexpensively. The problem (23) can be regarded as an ordinary differential equation with a matrix **A** as linear coefficient. Hence, we can explicitly give the solution of the initial value problem as

$$\mathbf{e}(t) = \exp(\tau\mathbf{A})\mathbf{e}_0, \quad \tau = t - t_0. \tag{24}$$

The matrix exponential is defined as

$$\exp(\mathbf{M}) = \sum_{j=0}^{\infty} \frac{\mathbf{M}^j}{j!}. \tag{25}$$

Recalling that $\mathbf{A}$, resulting e.g. from a FD discretization as depicted in Fig. 5, has at most 13 entries per row and a dimension n of approximately $3 \cdot N_x \times N_y \times N_z$, a direct evaluation of the matrix exponential seems not attractive. There is, however, an extensive theory behind the evaluation of functions involving matrices (Moler and Van Loan 2003).

For our purposes, another definition of the matrix exponential $\exp(\mathbf{A})$ is more useful. Let $\lambda_1, \lambda_2, \ldots, \lambda_n$ denote the n eigenvalues of $\mathbf{A}$, then it can be shown that the matrix exponential has a representation in the form of a polynomial p_{n-1} of degree $n - 1$, which interpolates $\exp(\mathbf{A})$ at the eigenvalues of $\mathbf{A}$. Then

$$\exp(\mathbf{A}) = p_{n-1}(\mathbf{A}) \tag{26}$$

However, this nice feature can not be exploited since n is large, and the eigenvalues of $\mathbf{A}$ are unknown. We therefore approximate $\mathbf{e}(t)$ by

$$\mathbf{e}_m(t) = p_{m-1}(\tau\mathbf{A})\mathbf{e}_0 \tag{27}$$

where p_{m-1} is a polynomial of low degree $m - 1 \ll n$.

A further, equivalent formulation is motivated by the appearance of the matrix product in the series (25). Consider the m-dimensional subspace of the n-dimensional space generated by the matrix $\mathbf{A}$ and the initial field $\mathbf{e}_0$,

$$\mathcal{K}_m(\mathbf{A}, \mathbf{e}_0) := \mathrm{span}\{\mathbf{e}_0, \mathbf{A}\mathbf{e}_0, \ldots, \mathbf{A}^{m-1}\mathbf{e}_0\}. \tag{28}$$

The construction of a Krylov subspace basis $\mathbf{V}_m := [\mathbf{v}_1, \mathbf{v}_2, \ldots, \mathbf{v}_m]^\top$ of $\mathcal{K}_m(\mathbf{A}, \mathbf{e}_0)$ can be achieved by the Lanczos process (Paige 1980), which is based on the three-term recurrence relation $\mathbf{A}\,\mathbf{v}_i = \beta_{i+1}\mathbf{v}_{i+1} + \alpha_i\mathbf{v}_i + \beta_i\mathbf{v}_{i-1}$, namely:

Let $\beta_1\mathbf{v}_1 = \mathbf{e}_0$. Then for $i = 1, 2, \ldots$ we have

$$\begin{aligned} \mathbf{w}_i &:= \mathbf{A}\mathbf{v}_i - \beta_i\mathbf{v}_{i-1} \\ \alpha_i &:= (\mathbf{v}_i, \mathbf{w}_i) \\ \beta_{i+1}\mathbf{v}_{i+1} &:= \mathbf{w}_i - \alpha_i\mathbf{v}_i \end{aligned}$$

with $(\cdot, \cdot)$ denoting the scalar product. In each step, β_i is determined from the condition that $(\mathbf{v}_i, \mathbf{v}_i) = 1$ for $i \geq 1$. The Krylov subspace basis $\mathbf{V}_m \in \mathbb{C}^{n\times m}$ satisfies

$$\mathbf{A}\mathbf{V}_m = \mathbf{V}_m\mathbf{T}_m + \beta_{m+1}\mathbf{v}_{m+1}\xi_m^\top. \tag{29}$$

When $\mathbf{A}$ is Hermitian, $\mathbf{T}_m = tridiag(\beta_i, \alpha_i, \beta_{i+1})$ is a tridiagnoal complex symmetric $m \times m$ matrix. ξ_m denotes the m-th column of the $m \times m$ identity matrix.

For our purposes, the matrix $\mathbf{A}$ is compressed by $\mathbf{T}_m = \mathbf{V}_m^\top\mathbf{A}\mathbf{V}_m$. The initial vector $\mathbf{e}_0$ is compressed in a similar way as $\mathbf{c} = \mathbf{V}_m^\top\mathbf{e}_0$. After evaluation of the low dimensional problem, the result is lifted up to the original space by

$$\mathbf{e}_m(t) = \mathbf{V}_m \exp(\tau\mathbf{T}_m)\mathbf{c}. \tag{30}$$

This method is known as the Spectral Lanczos Decompostion Method (Druskin and Knizhnerman 1988, 1989, 1994; Druskin et al. 1999). The matrix exponential has to be

evaluated only for the small matrix $\mathbf{T}_m$, as depicted in Fig. 11. For a summary of available numerical implementations of the matrix exponential for small m, see Moler and Van Loan (2003). Since no discretization in time is necessary, the size of the time step can be chosen arbitrarily (Fig. 12). However, the choice of τ becomes critical, when the conductivity of the medium is small, as will be explained later.

The convergence of the Krylov approximation to $\exp(\tau\mathbf{A})$ depends on the spectral properties of $\mathbf{A}$. As a rule of thumb, m should be chosen such that

$$m \approx \Delta_{\min}^{-1}\sqrt{\frac{\tau}{\mu\sigma_{\min}}}. \tag{31}$$

As m gets large, as would be the case when considering a low conductivity environment, storage of $\mathbf{V}_m$ may become expensive. For the comparably small sample FD matrix depicted in Fig. 5, there would be $\mathbf{V}_m \in \mathbb{R}^{239004\times m}$, which, for $m = 600$ and double precision arithmetics, would already result in a storage requirement of approx. 1 GB RAM. The restarted Krylov subspace algorithm proposed by Eiermann and Ernst (2006) proceeds by repeatedly generating a basis of Krylov spaces of fixed dimension m, updating the most recent approximation to (24), and then discarding all but the last basis vector, which is subsequently used as the initial vector for the next Krylov space. A modification proposed by Afanasjew et al. (2008) improved efficiency by replacing the matrix exponential with a rational approximation.

2.2.4 *Fourier Transform Based Methods*

An inverse Fourier transform of numerical results obtained by a frequency-domain code can also provide time-domain solutions. Newman et al. (1986) have presented examples for 3-D bodies embedded in horizontally layered media. Gupta et al. (1989) have computed time-domain responses by transforming frequency-domain solutions obtained by the Compact or Hybrid Finite Element Method back into the time-domain.

For a suitable number n_f of logarithmically equidistant frequencies 3-D frequency responses have to be transformed into the time-domain. As commonly agreed, the

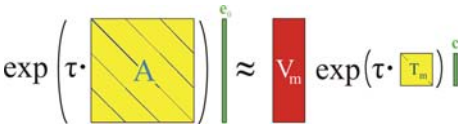

Fig. 11 The evaluation of the low dimensional problem involves only little numerical effort

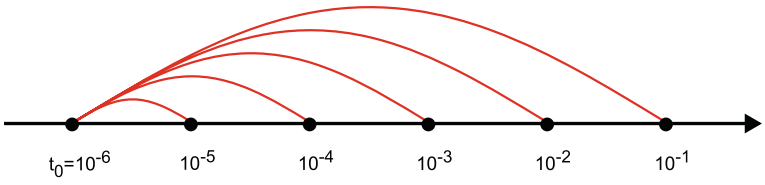

Fig. 12 Time steps in methods of SLDM type can be chosen arbitrarily, since a discretization in time is not required

requirement of n_f 3-D forward models is a daunting feature of this approach, unless the performance of 3-D solution would be remarkably boosted.

Mulder et al. (2008) have studied the numerical complexity of Fourier transforming multiple frequency-domain responses into the time-domain. With a highly convergent multigrid solver it was possible to demonstrate that the Fourier approach asymptotically performs better than time stepping algorithms, provided that the number of desired frequency-domain solutions n_f is small relative to the problem size n.

Börner et al. (2008) have proposed a variant using a model reduction technique in the frequency domain (MRFD). The inverse of the system matrix arising from a 3-D FE discretization of the time-harmonic Helmholtz equation has been projected onto a Krylov subspace, whose orthonormal basis has been generated using an Arnoldi process. The frequency-domain solutions have been obtained by solving a system of linear equations with a substantially lower dimension $m \ll n$ for a sweep of frequencies required by a Fast Hankel Transform. The transformation into the time-domain required only negligible numerical effort.

3 Equation Solvers

There have been published a great number of successful attempts to efficiently solve linear equation systems of the form (12) or (22) arising from the spatial discretization of the underlying partial differential equations using FD or FE methods. However, particularly for 3-D problems, these systems of linear equations become very large. Until recently, only iterative Krylov subspace methods of the conjugate gradient (CG) type were able to solve large equation systems with reasonable numerical effort. The convergence of a Krylov subspace iterative method can substantially be enhanced by applying an appropriate preconditioner, e.g. utilizing LU or Cholesky factorizations (Saad 2003). When such preconditionig techniques are applied, additional requirements for storing these complex-valued system matrices and factors become critical. To reduce the storage costs, Weiss (2001) successfully implemented a matrix-free variant of a conjugate gradient type solver. All Krylov subspace iterative solvers have in common that they do not need explicit storage of the system matrices. In fact, only the action of the matrix on a vector is required. The only tradeoff is the one between floating point operations for computing the necessary matrix elements versus memory management efficiency for large matrix arrays.

Recently, a revival of efficient direct solvers has been observed (Gould et al. 2007). These sparse matrix solvers are essentially of the Gauss elimination type, but highly optimized in terms of speed and memory requirements. Sparse direct methods solve systems of linear equations by factorizing the coefficient matrix, generally employing graph models to try and minimize both the storage needed and work performed. Sparse direct solvers have a number of common phases, which may be subdivided into

1. an ordering phase that exploits structure,
2. an analysis phase that investigates the matrix structure to determine a pivot sequence and data structure for efficient factorization,
3. a factorization phase that uses the previously determined pivot sequence to factorize the matrix,
4. a solve phase that performes forward elimination followed by back substitution using the stored factors.

The factorization is usually the most time-consuming phase, while the solve phase is significantly faster.

Consider the solution of the sparse system $\mathbf{Ax} = \mathbf{b}$. Using an explicit LU factorization into the product of a lower triangular matrix $\mathbf{L}$ and an upper triangular matrix $\mathbf{U}$ given by $\mathbf{A} = \mathbf{LU}$, the solution vector $\mathbf{x}$ may be obtained by a forward elimination followed by an inexpensive back substitution step given by

$$\mathbf{Ly} = \mathbf{b} \tag{32a}$$

$$\mathbf{Ux} = \mathbf{y}. \tag{32b}$$

An appealing feature of this approach is that multiple right-hand sides may easily be handled by sparse direct solvers. In terms of efficiency, there is little to distinguish between the leading competitors, e.g. PARDISO (Schenk and Gärtner 2004), and MUMPS (Amestoy et al. 2006).

In many cases, direct methods are the method of choice because finding and computing a good preconditioner for an iterative method can be computationally more expensive than using a direct method.

While iterative methods seem daunting for 3-D problems, recent advances in multigrid (MG) methods for the curl-curl operator (Reitzinger and Schoeberl 2002; Aruliah and Ascher 2003; Hiptmair and Xu 2006; Greif and Schötzau 2007; Mulder 2008; Haber and Heldmann 2007) may make this a viable option for large scale electromagnetic problems. Multigrid methods solve partial differential equations on a hierarchy of nested spatial discretizations. MG methods are among the fastest solution techniques known today (Hackbusch 1985). Common feature of MG methods is that a hierarchy of grids is considered. The important steps of MG are *Smoothing*, *Restriction*, and *Prolongation*.

Consider a linear system given on a fine grid. Usually, a few iterations of a Gauss–Seidel relaxation method effectively damp out high-frequency residual error components. The residual error associated with this approximate smooth solution will be downsampled (restricted) onto the next coarser grid. Since low-frequency error components on the fine grid correspond to high-frequency errors on the coarse grid, a structure similar to the original problem defined on the finer grid, but with essentially lower dimension, can be established on the coarse grid. This cycle (the *V-cycle*) will be repeated until the coarsest grid is reached. On the latter, the resulting small linear equation system can finally be solved using a direct solver. The obtained residual error has to be prolonged back to the finer grids. Eventually, with the approximation of the residual error on the finest grid the solution can be corrected.

Despite their promising optimality, MG methods are not common in the geophysical literature. A possible reason for this observation may be the fact that the MG methods are rather young, and their numerical implementation is not trivial. Coarse grids, prolongation and restriction operators have to be adjusted thoroughly with respect to the nature of the discretized region and the discretized differential equation.

4 Outlook

As has been stated by Avdeev (2005), the ultimate goal of 3-D modellers is the design of a highly accurate approximation to Maxwell's equations without adding more and more grid nodes within a computational domain under consideration. However, even for moderately dense grids, a typical 3-D modelling requires huge memory and remarkable computational

capacities. There are three possible ways to increase the performance of a given software code:

1. Increase the computing performance by use of faster processors.
2. Use better and optimized algorithms.
3. Use resources of many computing systems at a time.

Most modern CPUs already offer multi-core architecture, however, using today's conventional technology, the gain in performance is physically limited.

Over the last decade we have witnessed a dramatic boost in the performance and efficiency of numerical algorithms which evolved from huge efforts made in the theory of numerical mathematics.

With the availability of inexpensive desktop computers, software tools for the implementation of parallelized codes have been on the rise. The setup of ad-hoc clusters on the basis of conventional network connections requires only little technical and administrative effort. Software tools for the development of parallel codes are freely available. The Message Passing Interface (MPI) has become the de facto standard for communication among processes that model a parallel program running on a distributed memory system as well as on computing clusters (Snir et al. 1995). There are many points of departure for parallelization strategies:

– Solve Maxwell's equations for several frequencies and/or several transmitter positions independently in parallel.
– Decompose the computational domain into subdomains, solve small scale subproblems in parallel, and pass variables between nodes using message passing routines.
– Make use of parallel linear system solvers such as MUMPS and PARDISO.

Doubtlessly, there is much to be expected in the field of numerical methods in geo-electromagnetics, particularly when considering the recent boost in hardware speed and performance. Across the board, 3-D inversion codes are valuable interpretation tools. However, the numerical engine driving those inversion algorithms is mostly dominated by the forward operator. To efficiently solve a large number of linear equation systems arising from the problem discretization as well as for the sensitivity calculation, excellent libraries for the direct solution of linear systems using a matrix factorization are available. Some of these libraries are already prepared for parallel applications. Moreover, for a flexible discretization of geometries such as bathymetry or topography, the finite element method together with adaptive mesh refinement strategies will probably gain wide influence.

It is beyond question that the near future requires a change of paradigms in the development of numerical applications for the solution of geo-electromagnetic problems. Particularly, huge effort in the parallelization of existing codes will be expended, which is not only a challenging approach but also an ambitious task to meet both scientific and industrial requirements.

Acknowledgments My sincere thanks go to the Program Committee of the Beijing workshop, who offered me a chance to prepare and deliver this review. I would also like to thank the LOC and the German Science Foundation for funds to attend the workshop. I remain especially grateful to my colleagues Klaus Spitzer, Oliver G. Ernst, Michael Eiermann, and numerous students at Technische Universität Bergakadamie Freiberg for the incomparably wonderful teamwork. Suggestions from two anonymous reviewers greatly improved the manuscript.

References

Afanasjew M, Eiermann M, Ernst O, Güttel S (2008) Implementation of a restarted Krylov subspace method for the evaluation of matrix functions. Linear Algebra Appl 429:2293–2314

Amestoy P, Guermouche A, L'Excellent J-Y, Pralet S (2006) Hybrid scheduling for the parallel solution of linear systems. Parallel Comput 32(2):136–156

Aruliah D, Ascher U (2003) Multigrid preconditioning for Krylov methods for time-harmonic Maxwell's equations in 3D. SIAM J Sci Comput 24(2):702–718

Avdeev D (2005) Three-dimensional electromagnetic modelling and inversion from theory to application. Surv Geophys 26:767–799

Babuska I, Rheinboldt WC (1978) Error estimates for adaptive finite element computations. SIAM J Numer Anal 18:736–754

Badea E, Everett M, Newman G, Biro O, (2001) Finite-element analysis of controlled-source electromagnetic induction using Coulomb-gauged potentials. Geophysics 66(3):786–799

Bérenger JP. (1994) A perfectly matched layer for the absorption of electromagnetic waves. J Comput Phys 114(2):185–200

Börner RU, Ernst OG, Spitzer K (2008) Fast 3D simulation of transient electromagnetic fields by model reduction in the frequency domain using Krylov subspace projection. Geophys J Int 173(3):766–780

Coggon JH (1971) Electromagnetic and electrical modeling by the finite element method. Geophysics 36(1):132–155

Commer M, Newman G (2004) A parallel finite-difference approach for 3D transient electromagnetic modeling with galvanic sources. Geophysics 69(5):1192–1202

Davydycheva S, Druskin V, Habashi T, (2003) An efficient finite-difference scheme for electromagnetic logging in 3D anisotropic inhomogeneous media. Geophysics 68:1525–1536

Demkowicz L, Pal M (1998) An infinite element for Maxwell's equations. Comput Methods Appl Mech Eng 164:77–94

Dey A, Morrison H (1979) Resistivity modeling for arbitrarily shaped three-dimensional structures. Geophysics 44:753–780

Druskin VL, Knizhnerman LA (1988) Spectral differential-difference method for numeric solution of three-dimensional nonstationary problems of electric prospecting. Izvestiya Earth Phys 24:641–648

Druskin VL, Knizhnerman LA (1989) Two polynomial methods of calculating functions of symmetric matrices. USSR Comput Math Math Phys 29: 12–121

Druskin VL, Knizhnerman LA (1994) Spectral approach to solving three-dimensional Maxwell's diffusion equations in the time and frequency domains. Radio Sci 29:937–953

Druskin VL, Knizhnerman LA, Lee P (1999) New spectral Lanczos decomposition method for induction modeling in arbitrary 3-D geometry. Geophysics 64:701–706

DuFort EC, Frankel SP (1953) Stability conditions in the numerical treatment of parabolic differential equations. Math Tables Other Aids comput (former title of Math Comput) 7:135–152

Eiermann M, Ernst OG (2006) A restarted Krylov subspace method for the evaluation of matrix functions. SIAM J Numer Anal 44:2481–2504

Franke A, Börner RU, Spitzer K (2007) Adaptive unstructured grid finite element simulation of two-dimensional magnetotelluric fields for arbitrary surface and seafloor topography. Geophys J Int 171(1):71–86

Givoli D, (1992) Numerical methods for problems in infinite domains. Elsevier, Amsterdam

Givoli D (1999) Recent advances in the DtN FE method. Arch Comput Methods Eng 6(2):71–116

Gould NIM, Scott JA, Hu Y (2007) A numerical evaluation of sparse direct solvers for the solution of large sparse symmetric linear systems of equations. ACM Trans Math Softw 33(2):10

Greif C, Schötzau D (2007) Preconditioners for the discretized time-harmonic Maxwell equations in mixed form. Numer Linear Algebra Appl 14(4):281–297

Gupta PK, Raiche AP, Sugeng F (1989) Three-dimensional time-domain electromagnetic modelling using a compact finite-element frequency-stepping method. Geophys J Int 96(3):457–468

Haber E, Ascher UM (2001) Fast finite volume simulation of 3D electromagnetic problems with highly discontinuous coefficients. SIAM J Sci Comput 22(6):1943–1961

Haber E, Heldmann S (2007) An octree multigrid method for quasi-static Maxwell's equations with highly discontinuous coefficients. J Comput Phys 223(2):783–796

Haber E, Ascher U, Aruliah D, Oldenburg D (2000) Fast simulation of 3D electromagnetic problems using potentials. J Comput Phys 163(1):150–171

Haber E, Oldenburg D, Shekhtman R (2006) Rapid forward modelling of multi- source TEM data. In: Proceedings of the 4th international symposium on three- dimensional electromagnetics (3DEM-4). SEG

Haber E, Oldenburg D, Shekhtman R (2007) Inversion of time domain threedimensional electromagnetic data. Geophys J Int 171(2):550–564
Hackbusch W (1985) Multi-grid methods and applications. Springer, Berlin
Hiptmair R, Xu J (2006) Nodal auxiliary space preconditioning in H(curl) and H(div) spaces (Tech. Rep. No. 2006-09). ETH Zürich: Seminar für AngewandteMathematik.
Jin J, Zunoubi M, Donepudi KC, and Chew WC (1999) Frequency-domain and timedomain finite-element solution ofMaxwell's equations using spectral Lanczos decomposition method. Comput Methods Appl Mech Eng 169:279–296
Jones F, Pascoe L (1971) A general computer program to determine the perturbation of alternating electric currents in a two-dimensional model of a region of uniform conductivity with an embedded inhomogeneity. Geophys J Int 24:3–30
Key K, Weiss C (2006) Adaptive finite-element modeling using unstructured grids: the 2D magnetotelluric example. Geophysics 71(6):G291–G299
Kong FN, Johnstad SE, Rosten T, Westerdahl H (2008). A 2.5D finite-elementmodeling difference method for marine CSEM modeling in stratified anisotropic media. Geophysics 73(1):F9–F19
Livelybrooks D (1993) Program 3D feem: a multidimensional electromagnetic finite element model. Geophys J Int 114:443–458
Mackie RL, Madden TR, Wannamaker PE (1993) Three-dimensional magnetotelluric modeling using difference equations—theory and comparisons to integral equation solutions. Geophysics 58:215–226
Martinec Z, Everett ME, Velimsky J (2003). Time-domain, spectral-finite element approach to transient two-dimensional geomagnetic induction in a spherical heterogoeneous earth. Geophys J Int 155(1): 33–43
Mitsuhata Y, Uchida T (2004) 3D magnetotelluric modeling using the T-Omega finiteelement method. Geophysics 69(1):108–119
Moler C, Van Loan C (2003) Nineteen dubious ways to compute the exponential of a matrix, twenty-five years later. SIAM Rev 45(1):3–49
Monk P (1993) An analysis of Nédélec's method for the spatial discretization ofMaxwell's equations. J Comput Appl Math 47(1):101–121
Monk P (2003) Finite element methods for Maxwell's equations. Oxford University Press, New York
Moskow S, Druskin V, Habashy T, Lee P, Davydycheva S (1999) A finite difference scheme for elliptic equations with rough coefficients using a Cartesian grid nonconforming to interfaces. SIAM J Numer Anal 36(2):442–464
Mulder WA (2008) Geophysical modelling of 3D electromagnetic diffusion with multigrid. Comput Vis Sci 11(3):129–138
Mulder WA, Wirianto M, Slob EC (2008) Time-domain modeling of electromagnetic diffusion with a frequency-domain code. Geophysics 73(1):F1–F8
Nam MJ, Kim HJ, Song Y, Lee TJ, Son JS, Suh JH (2007) 3D magnetotelluric modelling including surface topography. Geophys Prospect 55(2):277–287
Nédélec J-C (1980) Mixed finite elements in R3. Numer Math 35:315–341
Nédélec J-C (1986) A new family of mixed finite elements in R3. Numer Math 50:57–81
Newman GA, Alumbaugh DL (1995) Frequency-domain modeling of airborne electromagnetic responses using staggered finite differences. Geophys Prospect 43:1021–1042
Newman GA, Hohmann GW, Anderson WL (1986) Transient electromagnetic response of a three-dimensional body in a layered earth. Geophysics 51:1608–1627
Oristaglio ML, Hohmann GW (1984) Diffusion of electromagnetic fields into a two-dimensional earth: a finite-difference approach. Geophysics 49:870–894
Paige CC (1980) Accuracy and effectiveness of the Lanczos algorithm for the symmetric eigenproblem. Linear Algebra Appl 34:235–258
Pain C, Herwanger J, Worthington M, Oliveira de C (2002) Effective multidimensional resistivity inversion using finite-element techniques. Geophys J Int 151(3):710–728
Potts D, Steidl G, Tasche M (2001). Fast Fourier transforms for nonequispaced data: a tutorial. In: Benedetto J, Ferreira P (eds) Modern sampling theory: mathematics and applications. Birkhauser, Boston
Pridmore DF, Hohmann GW, Ward SH, Still WR (1981) An investigation of finite-element modeling for electrical and electromagnetic data in three dimensions. Geophysics 46:1009–1024
Reddy IK, Rankin D, Phillips RJ (1977) Three-dimensional modelling in magnetotelluric and magnetic variational sounding. Geophys J Int 51:313–325
Reitzinger S, Schoeberl J (2002) An algebraic multigrid method for finite element discretizations with edge elements. Numer Linear Algebra Appl 9(3):223–238
Ruecker C, Guenther T, Spitzer K (2006). Three-dimensional modelling and inversion of DC resistivity data incorporating topography-I. Modelling. Geophys J Int 166(2):495–505

Saad Y (2003) Iterative methods for sparse linear systems, 2nd edn., Cambridge University Press
Schenk O, and Gärtner K (2004) Solving unsymmetric sparse systems of linear equations with PARDISO. J Future Gener Comput Syst 20(3):475–487
Smith JT, Booker JR (1991) Rapid inversion of two- and three-dimensional magnetotelluric data. J Geophys Res 96(B3):3905–3922
Snir M, Otto SW, Huss-Lederman S, Walker DW, Dongarra J (1995) MPI: the complete reference. MIT press, Cambridge
Spitzer K (1995) A 3D finite difference algorithm for DC resistivity modeling using conjugate gradient methods. Geophys J Int 123:903–914
Velimsky J, Martinec Z (2005) Time-domain, spherical harmonic-finite element approach to transient three-dimensional geomagnetic induction in a spherical heterogeneous earth. Geophys J Int 161(1):81–101
Wang T, Hohmann GW (1993) A finite-difference, time-domain solution for threedimensional electromagnetic modelling. Geophysics 58:797–809
Weidelt P (1999) 3D conductivity models: implications of electrical anisotropy. In: Oristaglio M, Spies B (eds) Three-dimensional electromagnetics. SEG, pp 119–137.
Weiss CJ (2001) A matrix-free approach to solving the fully 3D electromagnetic induction problem. SEG Tech Program Expand Abstr 20(1):1451–1454
Weiss CJ, Constable S (2006) Mapping thin resistors and hydrocarbons with marine EM methods, part II-modeling and analysis in 3D. Geophysics 71(6):G321–G332
Weiss CJ, Newman GA (2002) Electromagnetic induction in a generalized 3D anisotropic earth. Geophysics 67(3):1104–1114
Weiss CJ, Newman GA (2003) Electromagnetic induction in a generalized 3 anisotropic earth part 2 the LIN preconditioner. Geophysics 68(3):922–930
Yee KS (1966) Numerical solution of initial boundary problems involving Maxwell's equations in isotropic media. IEEE Trans Antennas Propag 14:302–309
Zienkiewicz OC, Taylor RL, Zhu JZ (2005) The finite element method: its basis & fundamentals, 6th edn. Elsevier, New York
Zunoubi MR, Jin JM, Donepudi KC, Chew WC (1999) A spectral lanczos decomposition method for solving 3-D low-frequency electromagnetic diffusion by the Finite-Element-method. IEEE Trans Antennas Propag 47:242–248
Zyserman FI, Santos JE (2000) Parallel finite element algorithm with domain decomposition for three-dimensional magnetotelluric modeling. J Appl Geophys 44:337–351